Diagn Interv Radiol 2015; 21: 466–470

CHEST IMAGING
ORIGINAL ARTICLE

Volumetric thin-section CT: evaluation of pulmonary interlobar fissures

Chun-Shuang Guan
Yan Xu
Dan Han
Jiang-Hong Chen
Xin-Lian Wang
Da-Qing Ma

PURPOSE
We aimed to perform an imaging analysis of interlobar fissures and their variations using thin-section computed tomography (CT).

METHODS
Volumetric thin-section CT scanning was performed in 208 subjects. Interlobar fissures were observed on axial images, and reconstructed coronal and sagittal images were observed by multiplanar reformatting (MPR). The vessel distributions were verified by maximal intensity projection (MIP). On the axial images, the interlobar fissures were characterized by lines of hyperattenuation, bands of hyperattenuation, avascular zones, and mixed imaging. The interlobar fissures were divided into seven grades according to the percentage of defects over the entire fissure.

RESULTS
On the axial images, of all interlobar fissures without avascular zones, 70.2% of the right oblique fissures (ROFs) and 94.2% of the left oblique fissures (LOFs) appeared as lines, and 83.2% of the horizontal fissures (HFs) appeared as bands. All of the interlobar fissures appeared as lines on the coronal and sagittal images. Of all cases, 17.8% showed fully complete interlobar fissures for all three fissures. Incomplete fissures included 41.3% of ROFs, 58.2% of HFs, and 45.2% of LOFs. In ROFs and LOFs, discontinuity was most frequently below 20%, while in HFs discontinuity was most frequently 41%–60%. The most common classification of incomplete interlobar fissures was a discontinuous avascular zone.

CONCLUSION
Incomplete interlobar fissures are common variations of interlobar fissures. Techniques including volumetric thin-section CT, MPR, and MIP can assist in the diagnosis of incomplete interlobar fissures.

The pulmonary interlobar fissures are important landmarks for pulmonary anatomy. They adopt a double membrane structure formed by invagination of the visceral pleura. The interlobar fissures are 1–3 mm thick and consist of the right oblique fissure (ROF), horizontal fissure (HF), and left oblique fissure (LOF) (1, 2). The recognition of pulmonary interlobar fissures and their variations is beneficial for identifying pulmonary lesion locations, evaluating disease progression, selecting surgical operations, and applying endoscopic therapy (3–5). With the constant development of imaging techniques, thin-section computed tomography (CT) can provide more detailed information regarding lung structure with respect to the anatomy (5–7). Multiplanar reformatting (MPR) (8) and maximal intensity projection (MIP) are reconstruction techniques based on a noninvasive methodology that detect pulmonary interlobar fissure variations. The results generated by these techniques highly resemble the results of an autopsy (8). In this study, the pulmonary interlobar fissures and their variations were investigated and analyzed by volumetric thin-section MPR and MIP images.

Methods

The study was approved by the institutional review board and the institutional ethics committee. A retrospective analysis was performed on CT scans of 862 adult subjects (≥18 years) between February 2014 and April 2014. Patients with pulmonary diseases, pleural diseases, mediastinal lesions, and chest operations that involved the interlobar fissures were

From the Department of Radiology (C.S.G., Y.X., D.H., J.H.C., X.L.W., D.Q.M ✉ *madaqing00@163.com*) Beijing Friendship Hospital, Capital Medical University, Beijing, China; the Department of Radiology (C.S.G.), Beijing Fengtai Hospital, Beijing, China; the Department of Radiology (X.L.W.), Fu Xing Hospital, Capital Medical University, Beijing, China.

Received 26 February 2015; revision requested 19 March 2015; final revision received 24 April 2015; accepted 2 May 2015.

Published online 31 August 2015.
DOI 10.5152/dir.2015.15080

excluded. A total of 208 patients (18–88 years of age; mean age, 56±14 years) with normal or almost normal pulmonary conditions were selected for this study, including 106 females (25–88 years of age; mean age, 56±13 years) and 102 males (18–87 years of age; mean age, 55±15 years).

CT imaging

A 128-detector spiral CT scanner (Brilliance iCT, Philips) was used in the current study. The scans were obtained at end-inspiration using a single breath-hold technique in the supine position. Scans were obtained from the lung apex to the adrenal gland. The scan parameters were as follows: 120 kV tube voltage, 100 mAs tube current. Consecutive images were obtained with a slice thickness of 1.25 mm and an interval of 1.25 mm. The coronal and sagittal images (1 mm) were reconstructed by MPR to observe the interlobar fissures. Oblique images and slices of various thicknesses were also used for observation when necessary. The window settings included a width of 1000 Hounsfield Unit (HU) and a level of -500 HU. Other widths and levels were also used for the window setting if required.

Image evaluation

Two radiologists with 10 and 13 years of experience in thoracic imaging reviewed the CT scans. When a discrepancy occurred between the two radiologists, a consensual diagnosis was reached through discussion. In the axial CT, the morphologies of the interlobar fissures were represented as lines of hyperattenuation, bands of hyperattenuation, avascular zones, and mixed imaging of lines, bands, or avascular zones. Complete interlobar fissures were defined as continuous interlobar fissures that were attached to the hilar or mediastinal structures in any given slice. Incomplete interlobar fissures referred to discontinuous fissures or detachment from the hilum or mediastinum. In addition, the lung tissues in the region of discontinuous fissures merged into each other (3–5). Incompleteness of the interlobar fissures was expressed as a percentage of defects over the entire fissure and categorized into seven grades: grade 0, 0% incomplete (i.e., fully complete fissure); grade 1, 1%–20% incomplete; grade 2, 21%–40% incomplete; grade 3, 41%–60% incomplete; grade 4, 61%–80% incomplete; grade 5, 81%–99% incomplete; and grade 6, 100% incomplete (i.e., fissure is absent) (2, 4). The incomplete interlobar fissures were classified into four types (8): type 1, the interlobar fissure was a discontinuous avascular zone; type 2, blood vessels in the adjacent lobes crossed over the interlobar region; type 3, pulmonary blood vessels, especially the pulmonary vein, penetrated the interlobar region; and type 4, the pulmonary vein was observed in the interlobar region and was connected to the vessels in the adjacent lobes (Fig. 1). The fissure defects were classified as medial, intermediate, or lateral based on their localization. The classification of interlobar fissures with regard to their grade, type, and location of defects was based on axial CT images and coronal and sagittal MPR images. The fissures were also reconfirmed on oblique images if required. The vessel distribution could also be verified by MIP.

Main points

- On volumetric thin-section CT, most of the oblique fissures appeared as lines and horizontal fissures appeared as bands. However, all interlobar fissures appeared as lines on coronal and sagittal images.
- Only 17.8% of all cases had all three interlobar fissures fully complete.
- The defects of the interlobar fissures were frequently located near the hilar or mediastinal regions.
- The most common classification of incomplete interlobar fissures was a discontinuous avascular zone.
- Techniques including volumetric thin-section CT, multiplanar reformat, and maximal intensity projection can assist in the diagnosis of incomplete interlobar fissures.

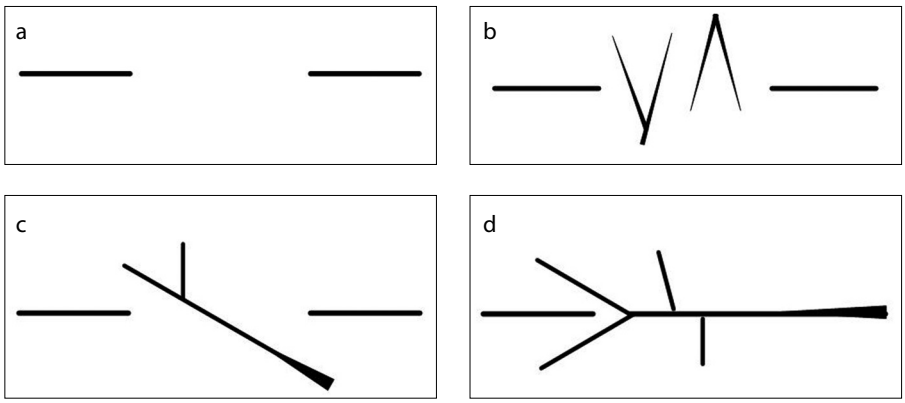

Figure 1. a–d. Classification of incomplete interlobar fissures. Type 1: the interlobar fissure is a discontinuous avascular zone **(a)**. Type 2: the vessel in the adjacent lobe intersects over the interlobar region **(b)**. Type 3: pulmonary blood vessel, especially the pulmonary vein, penetrates the interlobar region **(c)**. Type 4: the pulmonary vein is observed in the interlobar region and is attached to the vessels in the adjacent lobe **(d)**.

Statistical analysis

SPSS 17.0 (SPSS Inc.) was used for the statistical analysis. Descriptive statistics were used to report various ratios of interlobar fissure assessment. The agreement between the two radiologists was analyzed using the weighted κ index. The criteria were as follows: $\kappa \leq 0.2$, slight agreement; $0.2 < \kappa \leq 0.4$, fair agreement; $0.4 < \kappa \leq 0.6$, moderate agreement; $0.6 < \kappa \leq 0.8$, substantial agreement; and $\kappa > 0.8$, nearly perfect agreement. The differences between interlobar fissure grades were examined with the Kruskal-Wallis test. The remaining data were evaluated using the chi-square test. A value of $P < 0.05$ suggests a statistically significant difference. For triplicate comparisons, a value of $P < 0.017$ indicates a statistically significant difference.

Results

Agreement between the two radiologists was fair to nearly perfect (Table 1). The average κ values for the agreements regarding ROFs, HFs, and LOFs were 0.646, 0.652, and 0.593, respectively ($P = 0.825$).

On reconstructed coronal and sagittal MPR images, all interlobar fissures appeared as lines (Fig. 2), and the HFs were particularly clear, which was beneficial for the evaluation of the interlobar fissures (Table 2).

Table 1. Interobserver agreement κ indices

Fissures	Morphology	Defects	Grade	Type
ROF	0.608 (n=208, $P < 0.001$)	0.661 (n=86, $P < 0.001$)	0.851 (n=208, $P < 0.001$)	0.465 (n=86, $P < 0.001$)
HF	0.474 (n=199, $P < 0.001$)	0.726 (n=121, $P < 0.001$)	0.774 (n=208, $P < 0.001$)	0.632 (n=121, $P < 0.001$)
LOF	0.431 (n=207, $P < 0.001$)	0.650 (n=94, $P < 0.001$)	0.763 (n=208, $P < 0.001$)	0.528 (n=94, $P < 0.001$)

ROF, right oblique fissure; HF, horizontal fissure; LOF, left oblique fissure.

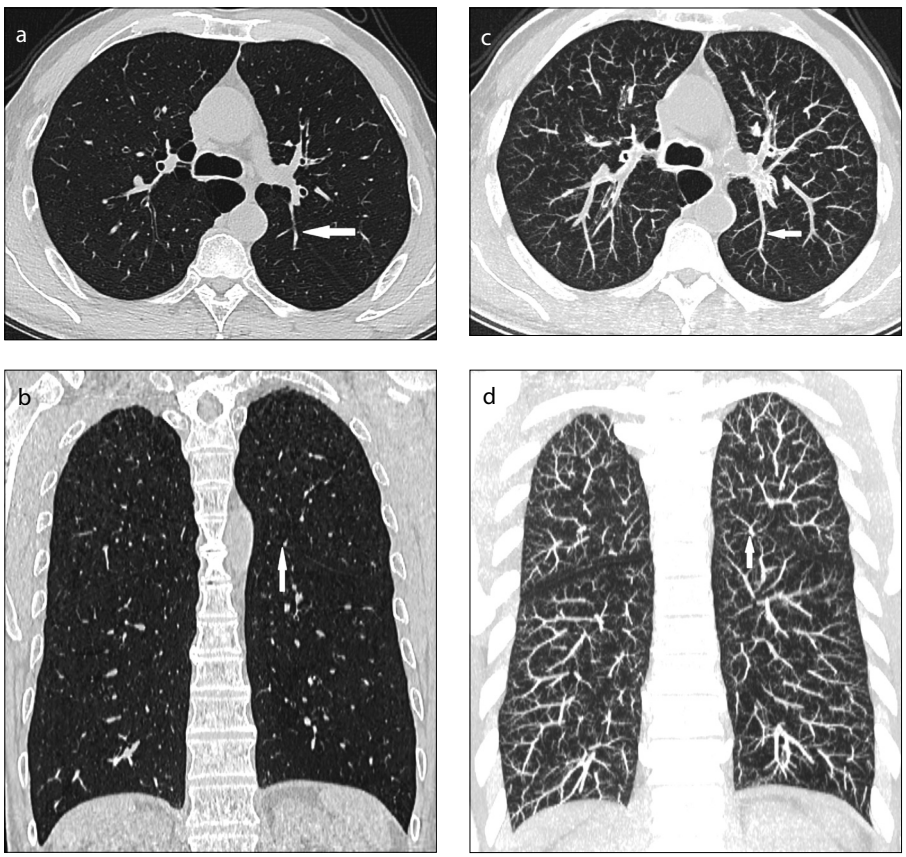

Figure 2. a–d. A 54-year-old man with pulmonary bulla. Axial image **(a)** shows the left oblique fissure appearing as a band of hyperattenuation. Coronal image **(b)** shows the left oblique fissure appearing as a line of hyperattenuation. Axial **(a, c)** and coronal **(b, d)** images show the left lung presenting with medial incompleteness in the left oblique fissure *(white arrow)*. Maximal intensity projection images **(c, d)** show a branch of the apicoposterior segmental vein penetrating the interlobar region, indicating a Type 3 fissure.

In total, 58.7% of ROFs, 37.5% of HFs, and 54.3% of LOFs were fully complete. Of the cases, 17.8% (37/208; 16 females and 21 males) had fully complete fissures in all three types. Grades 1 to 5 represented incomplete interlobar fissures and included 48.2% of the fissures (301/624; 151 in females and 150 in males). The incomplete interlobar fissures comprised 41.3% ROFs, 58.2% HFs, and 45.2% LOFs (Table 2). Grades of incompleteness was significantly different between HFs and ROFs and between HFs and LOFs (Kruskal Wallis test, $P < 0.001$ for both comparisons) but not between ROFs and LOFs ($P = 0.032$ [$P > 0.017$]).

Among 301 incomplete interlobar fissures, 93.7% (282/301) were located peripheral to the hilum or mediastinum, while 6.3% (19/301) showed defects in the intermediate region. No cases presented lateral fissure defects. Intermediate defects were only observed in HFs and were clearly observed in the coronal and sagittal images (Table 2). Location of interlobar fissure defects was significantly different between HFs and ROFs and between HFs and LOFs (chi-square test, $P < 0.001$ for both), but not between ROFs and LOFs ($P = 0.684$).

With regard to the classification of incomplete interlobar fissures, MIP images showed the presence of vessels and their origins and directions, which helped radiologists to distinguish the types of defects. Type 1 was the most frequently observed defect type and was present in 36.2% of the fissures (109/301), followed by type 4 (23.9%, 72/301), type 3 (22.6%, 68/301), and type 2 (17.3%, 52/301). Type 1 was the mostly commonly observed defect type in ROFs (Fig. 2). In HFs, types 1, 3, and 4 were observed at nearly equal proportions (Fig. 3). Type 1 was the most commonly observed defect in LOFs, and types 2 and 4 were observed in nearly equal proportions (Table 2). MPR and MIP images were used to assist in identification of the blood vessel origin and direction (Figs. 2 and 3). Distribution of defect types was significantly different between HFs and ROFs and between HFs and LOFs (chi square test, $P = 0.007$ for HFs-ROFs, $P = 0.001$ for HFs-LOFs), but not between ROFs and LOFs ($P = 0.472$).

Discussion

Our study showed that incomplete fissures (48.2%) were common variations in interlobar fissures, and none of the fissures appeared as avascular zones on thin-section CT. Moreover, all interlobar fissures appeared as lines on coronal and sagittal views, which were especially suitable for the observation of HFs. Grading of interlobar fissure defect severity showed that greater defects were encountered in lesser frequencies.

The pulmonary interlobar fissures divide the lung into the right superior/middle/inferior lobes and the left superior/inferior lobes. The appearance of interlobar fissures on CT can be represented as avascular zones, bands of hyperattenuation, and lines of hyperattenuation. On a standard CT scan with 10 mm thick sections, the ratios of avascular zones, lines, and bands were 60%–94%, 1%–18%, and 0%–8%, respectively, for ROFs; 58%–82%, 1%–22%, and 0%–18%, respectively, for LOFs (3, 9). In addition, on a high-resolution CT or a thin-section CT scan with 1–2 mm thick

Table 2. Imaging findings of interlobar fissures

	ROF (n=208)	HF (n=208)	LOF (n=208)	*P*
Morphology				
Lines	146 (70.2)	0	196 (94.2)	
Bands	0	173 (83.2)	0	<0.001
Mixed imaging	62 (29.8)	26 (12.5)	11 (5.3)	
Grading				
0	122 (58.7)	78 (37.5)	113 (54.3)	
1	73 (35.1)	44 (21.2)	50 (24.0)	
2	6 (2.9)	41 (19.7)	12 (5.8)	
3	2 (1)	23 (11.1)	8 (3.8)	<0.001
4	4 (1.9)	6 (2.9)	11 (5.3)	
5	1 (0.5)	7 (3.4)	13 (6.2)	
6	0	9 (4.3)	1 (0.5)	
Defect location				
Medial defect	86 (41.3)	102 (49.0)	94 (45.2)	<0.001
Intermediate defect	0	19 (9.1)	0	
Classification				
1	36 (17.3)	42 (20.2)	31 (14.9)	0.003
2	18 (8.7)	9 (4.3)	25 (12.0)	
3	17 (8.2)	35 (16.8)	16 (7.7)	
4	15 (7.2)	35 (16.8)	22 (10.6)	

Data are presented as n (%).
ROF, right oblique fissure; HF, horizontal fissure; LOF, left oblique fissure.

sections, the ratios of avascular zones, lines, and bands were 0%, 74%–94%, and 6%–18%, respectively, for ROFs; 0%, 96%–98%, and 2%–4%, respectively, for LOFs (1, 3, 4, 6). In this study, no avascular zone was observed in thin-section axial CT, and 70.2% of ROFs and 94.2% of LOFs were shown as lines, and 83.2% of HFs as bands. Therefore, it was clear that the interlobar fissures often appear as avascular zones on a standard CT (9, 10), while they often appear as lines on thin-section CT (1, 4, 6). The thin-section CT was beneficial for recognizing the fissures and resulted in a higher probability of the interlobar fissures being observed as lines and a lower probability of reporting avascular zones and bands. Moreover, it was important to evaluate the interlobar fissures on coronal and sagittal reformats, especially for HFs that appeared as lines and not bands. The morphologies of interlobar fissures may be relevant to factors such as the scan slice thickness, CT resolution, scan angle, and the directions of interlobar fissures (3, 6, 7, 10).

Based on several studies using high resolution CT (1.5 mm thick section) and thin-section CT (1–2 mm thick sections), the probability of having incomplete fissures can vary as 17.4%–87% for ROFs, 20.4%–86.9% for HFs, and 18.6%–70.4% for LOFs (4, 6, 8, 11–13). In this study, incomplete ROFs, HFs, and LOFs exhibited frequencies of 41.3%, 58.2%, and 45.2%, respectively. HFs are the most frequently observed incomplete fissures (5). Incompleteness has more often been observed in LOFs than in ROFs, and the incomplete regions of interlobar fissures are most often located medially, near the hilar region, or mediastinal region (12), which is in agreement with the present study. However, in this study, 9.1% of HFs were found to be discontinuous in the intermediate region, which might relate to the direction of HFs. In previous studies, among the four types of incomplete interlobar fissures, both ROFs and LOFs were most frequently observed as type 1, whereas HFs were most frequently observed as type 3 or type 4 (4, 8). In this study, the results for ROFs and LOFs indicated agreement with these studies, but the results for HFs were different, as similar probabilities were observed for HFs of types 1, 3, and 4. Thus, type 1 HFs can be observed just as frequently.

Grade 0 indicated fully complete interlobar fissures. Previous studies have indicated that the frequencies of fully complete fissures range as 37.5%–64.8% for ROFs, 22.40% for HFs, and 40.3%–75.6% for LOFs (2, 4), which are similar to the results of the present study. ROFs and LOFs were frequently shown as complete fissures. In this study, 17.8% of the cases demonstrated full integrity in all three types of interlobar fissure. There have been very few studies that show simultaneous completeness in all three fissures.

Grade 6 indicated an absence of interlobar fissures. A total of 3.0%–3.2% of HFs were observed as absent in previous studies (4, 11), and 4.3% were absent in this study. In addition, this study discovered one case with an absent LOF. In previous studies, the numbers of cases with grade 1–3 ROFs were similar. For HFs, the most frequently observed grade was grade 5. For LOFs, grade 2 was observed in the highest number of cases, whereas grades 4 and 5 were significantly less frequently observed (2, 4). In this study, the most frequently observed grade for ROFs, HFs, and LOFs was grade 1, which consisted of small gaps, and the least frequently observed grades included grades 3 to 5 for all three types of fissures.

One limitation was that no clinical relevance was discussed regarding pulmonary interlobar fissures in this study. However, previous valuable studies have investigated the clinical significance of the pulmonary interlobar fissures, including the location of pulmonary lesions, distribution of pleural effusion, dissemination of inflammation and tumors, selection of surgical operations, endoscopic therapy for severe emphysema, and the differential diagnosis between normal and pathological structures (5, 6).

In conclusion, incomplete interlobar fissures comprised 41.3% of ROFs, 58.2% of HFs, and 45.2% of LOFs. The defects were frequently located near the hilar or mediastinal region. The techniques of volumetric thin-section CT scanning, MPR, and MIP were beneficial for recognizing pulmonary interlobar fissures and their variations and establishing the grading and classification for incomplete interlobar fissures.

Acknowledgements

We are grateful to our colleagues in the Department of Radiology in Beijing Friendship Hospital. We thank American Journal Experts for providing language editing services.

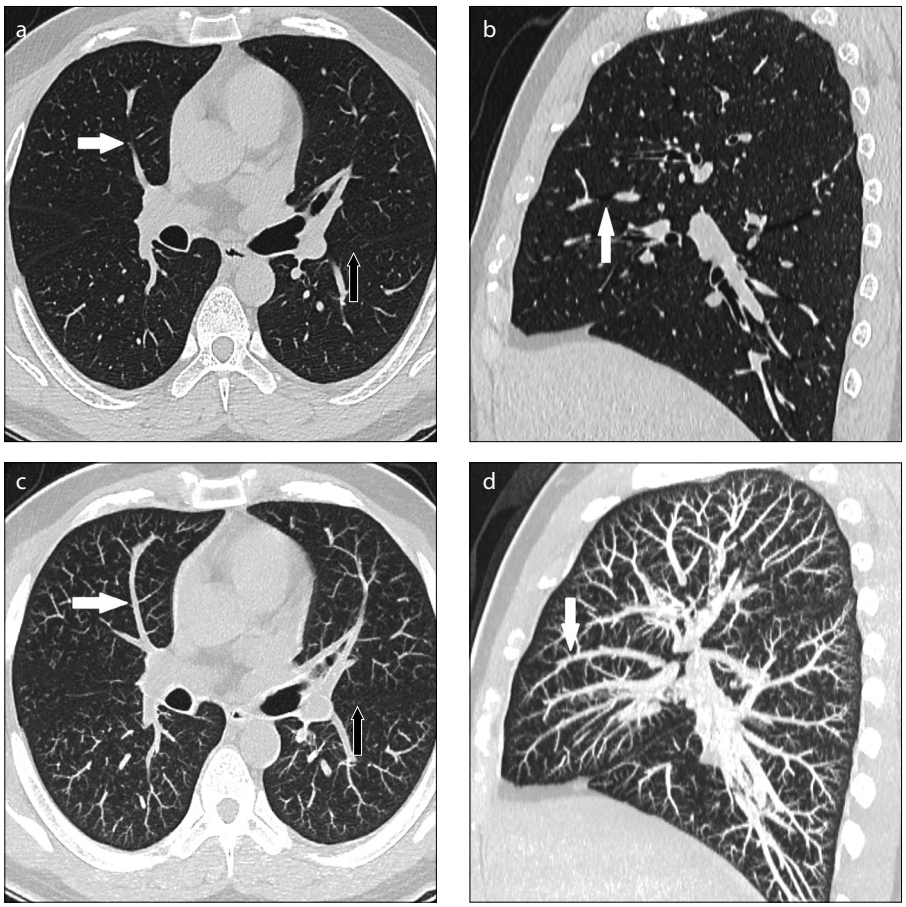

Figure 3. a–d. A 33-year-old man. Axial **(a, c)** and sagittal **(b, d)** images show the horizontal fissure in the right lung presenting with a medial defect *(white arrow)* and the left interlobar fissure presenting with medial incompleteness *(black arrow)*. Maximal intensity projection images **(c, d)** show that the vessel in the defect region was the medial vein in the middle lobe *(white arrow)* indicating a Type 4 fissure, and no vessel distribution in the defect region *(black arrow)* indicating a Type 1 fissure.

Conflict of interest disclosure

The author declared no conflicts of interest.

References

1. Aziz A, Ashizawa K, Nagaoki K, Hayashi K. High resolution CT anatomy of the pulmonary fissures. J Thorac Imaging 2004; 19:186–191. [CrossRef]
2. Gülsün M, Ariyürek OM, Cömert RB, Karabulut N. Variability of the pulmonary oblique fissures presented by high-resolution computed tomography. Surg Radiol Anat 2006; 28:293–299.[CrossRef]
3. Glazer HS, Anderson DJ, DiCroce JJ, et al. Anatomy of the major fissure: evaluation with standard and thin-section CT. Radiology 1991; 180:839–844. [CrossRef]
4. Heřmanová Z, Ctvrtlík F, Heřman M. Incomplete and accessory fissures of the lung evaluated by high-resolution computed tomography. Eur J Radiol 2014; 83:595–599. [CrossRef]
5. Koenigkam-Santos M, de Paula WD, Owsijewitsch M, et al. Incomplete pulmonary fissures evaluated by volumetric thin-section CT: semi-quantitative evaluation for small fissure gap identification, description of prevalence and severity of fissural defects. Eur J Radiol 2013; 82:2365–2370. [CrossRef]
6. Cronin P, Gross BH, Kelly AM, Patel S, Kazerooni EA, Carlos RC. Normal and accessory fissures of the lung: evaluation with contiguous volumetric thin-section multidetector CT. Eur J Radiol 2010; 75:e1–8. [CrossRef]
7. Schieman C, MacGregor JH, Kelly E, et al. Can preoperative computed tomography of the chest predict completeness of the major pulmonary fissure at surgery? Can J Surg 2011; 54:252–256. [CrossRef]
8. Mahmut M, Nishitani H. Evaluation of pulmonary lobe variations using multidetector row computed tomography. J Comput Assist Tomogr 2007; 31:956–960. [CrossRef]
9. Proto AV, Ball JB Jr. Computed tomography of the major and minor fissures. AJR Am J Roentgenol 1983; 140:439–448. [CrossRef]
10. Berkmen YM, Auh YH, Davis SD, Kazam E. Anatomy of the minor fissure: evaluation with thin-section CT. Radiology 1989; 170:647–651. [CrossRef]
11. Ariyürek OM. Anatomy of the minor fissure: assessment with high-resolution CT and classification. Eur Radiol 2002; 12:175–180. [CrossRef]
12. Frija J, Naajib J, David M, Hacein-Bey L, Yana C, Laval-Jeantet M. Incomplete and accessory pulmonary fissures studied by high resolution x-ray computed tomography. J Radiol 1988; 69:163–170.
13. Ozmen CA, Nazaroglu H, Bayrak AH, Senturk S, Akay HO. Evaluation of interlobar and accessory pulmonary fissures on 64-row MDCT. Clin Anat 2010; 23:552–558. [CrossRef]